Using mesoporous carbon to pack polyethylene glycol as a shape-stabilized phase change material with excellent energy storage capacity and thermal conductivity

Daili Feng[1,2,*], Pei Li[1], Yanhui Feng[1,2,*], Yuying Yan[3], Xinxin Zhang[1,2]

1. School of Energy and Environmental Engineering, University of Science and Technology Beijing, Beijing 100083, P.R. China

2. Beijing Key Laboratory of Energy Saving and Emission Reduction for Metallurgical Industry, School of Energy and Environmental Engineering, University of Science and Technology Beijing, Beijing 100083, P.R. China

3. Fluids & Thermal Engineering Research Group, Faculty of Engineering, University of Nottingham, Nottingham NG7 2RD, UK

Abstract

A novel shape-stabilized phase change material was successfully prepared using polyethylene glycol (PEG) as PCM and mesoporous carbon FDU-15 as support via the melting impregnation method. The structural and thermal properties of materials were measured by TEM, SEM, XRD, FT-IR, nitrogen adsorption-desorption isotherms and DSC, respectively. The maximum loading of PEG/FDU-15 reaches up to 75 wt%, and the corresponding crystallization ratio is 71%, which is superior to other mesoporous-based composite phase change materials. Molecular dynamic (MD) analysis showed that some PEG adhered to the pore wall with an amorphous structure which failed to crystallize, ultimately resulting in a gap between the measured latent heat and the theoretical value. It was interesting that the filling of PEG could stimulate the frequency shift of atomic vibration in FDU-15, which then just fell in the dominant vibrational zone of PEG, despite the suppressed atomic vibration of PEG after compounding. Accordingly, the thermal conductivity of the composite is more than 60% higher

Corresponding author. Tel: 008662332599. E-mail: yhfeng@me.ustb.edu.cn (Yanhui Feng), dlfeng@ustb.edu.cn (Daili Feng)

compared to pure PEG, which relates to the reinforced matching of the atomic vibration between the skeleton and PCM material. FDU-15 was applied to pack PCM for the first time and delivered a better thermal performance compared with other mesopore-based composite PCMs.

Keywords: polyethylene glycol; FDU-15; composite phase change material; thermal properties; molecular dynamics

1. Introduction

Energy storage technology is a way to achieve efficient use of energy, which can alleviate the mismatch between energy supply and demand[1]. There are mainly three ways of energy storage: sensible heat storage, latent heat storage, chemical reaction energy storage, among which the latent heat storage has become the most popular method because of the characteristics such as small temperature fluctuation, high energy storage density and wide range of phase change temperature, as well as easy operation and control in the process of energy storage. Researchers' attentions have been concentrated upon the fields of latent heat storage using phase change materials (PCM) to solve cutting-edge topics in renewable energy harvesting[2], chip cooling[3,4], thermal control in spacecraft[5,6] and so on. As the main function part, PCM plays a critical role in thermal energy storage, but it is very easy to leak out and corrode the surroundings during the solid-liquid phase change[7-10]. While the nanopore-based shape-stabilized composite (porous skeleton + PCM) has been regarded as one of the best ways to address the above issue. Capillary force enables the nanoporous skeleton to bind the PCM in the pores, so as to avoid leakage[11]. Besides, the nature of porous materials will be assigned to the associated composites, such as high thermal conductivity, highly flame retardancy, etc. In addition to the building[12]

and solar-thermal[13] fields which composite PCMs is commonly used, the guest-host interaction between the porous skeleton and PCM makes composites applicable to more other fields, including magnetic-thermal conversion[14], thermal management of electronics[15], medical[16] and etc. . At present, research on composite PCMs is mainly focused on the selection and optimization of substrates. For example, the substrates with smaller pore size (nanoscale), regular channels, and larger specific surface area, or porous frameworks that can enhance thermal and heat transfer performance (carbon-based) are preferred by researchers to encapsulate PCMs (Fig. 1).

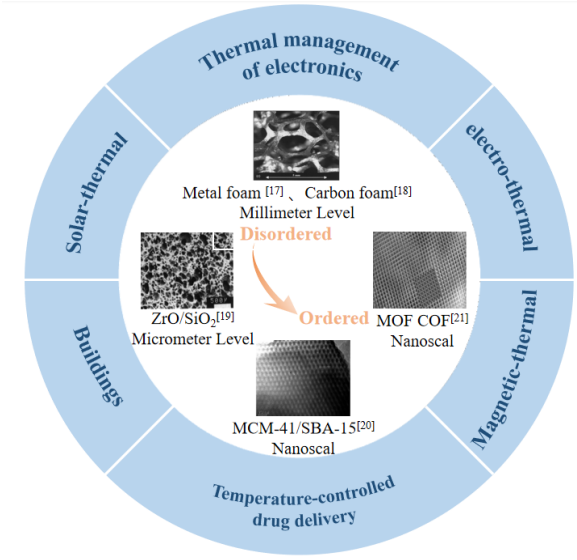

Fig. 1 Applications of composite PCMs and the evolution of porous skeleton[17-21]

Readily synthesized mesoporous materials are expected to be good candidates for packing PCMs as they possess high specific surface area and pore volume. Here we listed the results[22-24] of thermal properties for two commonly used PCMs (polyethylene glycol (PEG) and stearic acid (SA)) immobilized by mesoporous materials, as shown in Table 1. Most of the researches are concentrated on silica-based composites rather than carbon-based ones. For the ordered mesoporous carbon derived composite PCMs, CMK-3 fails to further increase the loading of SA with a maximum percentage of only 46 wt%[24], which might be attributed to the carbon rods arranged pore structure and the absence

of independent confined space for PCM. The maximum loading of the silicon-based composite PCM PEG/MCM-41(SBA-15) is 70 wt%[22,23]. But due to the strong interaction between the PEG molecular and MCM-41(SAB-15) skeleton, many PEG molecules attached to the inner surface of the skeleton without phase change, the surface functionalization on mesoporous silica is required to drive crystallization of PEG [22,23]. Yet thermal conductivities of these composites have rarely been collected, though it is critical for the rate of heat storage/release during practical usage.

Table 1 Shape-stabilized PCMs based on mesoporous materials

PCM	Mesoporous skeletons	Loading (wt%)	T_m/T_c (°C)	$\Delta H_m/\Delta H_c$ (J/g)	k (W/m·K)	Ref.
PEG	MCM-41-OH	70	--/--	0	--	[22]
	MCM-41-NH_2	60	50.76/--	58.76/--	0.24	
	HO-SBA-15-OH	70	--/--	0	--	[23]
	NH_2-SBA-15-CH_3	70	52/30	88.2/82.2	--	
SA	SBA-15	52	69.1/66.7	36.3/35.4	--	[24]
	CMK-3	46	82.9/78.9	31.5/26.5	--	

Actually, the thermal conductivity of carbon-based materials is believed to be superior to silica. So, mesoporous carbon FDU-15 is selected in this work as the first time to prepare a form-stable PCMs. It has a pore size of 2.6-6.8 nm and regular two-dimensional hexagonal pore structure, which is similar to mesoporous silica MCM-41 but in contrast with CMK-3, providing a basis for comparison. It has the characteristics of good thermal stability (1400°C), large specific surface area (968 m^2/g), uniform pore size and high thermal conductivity[25]. At present, the research on FDU-15 is mostly concentrated on the fields of adsorption and catalysis[26,27]. We choose PEG as PCM material, which has a suitable melting temperature (46°C-65°C) and high latent heat (145 J/g-175 J/g) during phase change progress. Existing studies have shown that the composite phase change material using PEG as PCM exhibits good thermal properties and therefore has a wide range of applications in thermal energy storage[28]. In this

paper, we prepared PEG/FDU-15 composites with different mass percentages and characterized their thermal properties. The phase change and heat transfer mechanism have been investigated by MD simulations. We expect to obtain composite phase change materials with excellent performance and also provide directional guidance for the design of such mesopore-based composite phase change materials.

2. Experimental

2.1 *Preparation*

FDU-15 was fabricated by XFNANO company, with a specific surface area ⩾600 m^2/g, and pore size of 4~6 nm. The PEG/FDU-15 composites were prepared by the melting impregnation method[29,30]. Firstly, PEG and FDU-15 were weighed according to a certain mass percentage and mixed in a 50 ml round bottom flask. Then absolute ethanol was added and 1/3 filled the flask. The suspension was placed in a constant temperature (70°C) water bath and stirred for about 3~4 h to mix well. Finally, the mixture was dried in an oven at 80°C until the ethanol was entirely evaporated.

2.2 *Characterization*

The X-ray diffraction (XRD) was measured by D/max-2500/PC using Cu Kα as the X-ray source. Transmission electron microscopy (TEM, JEM-2010) and scanning electron microscopy (SEM, ZEISS SUPRA55) was used to observe the structure of the skeleton and composites, respectively. The chemical structure analysis of the framework was carried out by Fourier transform infrared spectroscopy (FT-IR, PerkinElmer Spectrum 100). Nitrogen adsorption-desorption isotherms were performed with a surface area analyzer (Micromeritics ASAP 2460) at 77K, and the sample was degassed at 150°C under vacuum for 8 hours before testing. The specific surface area was calculated by the Brunauer-Emmett-Teller (BET) equation, and the pore size distribution was obtained by the Barret-Joyner-Halenda (BJH) model. Total pore volumes can be calculated by the amount adsorbed at a relative pressure of 0.98. In addition, the

maximum loading of the composite was tested by the solid-liquid phase change characteristics of PEG. We placed the obtained composite on a filter paper, heated it above the PEG phase change temperature (set to 80° C) and reserved it for 30 min. The leakage of PEG can be judged by observing whether there was oil on filter paper. The melting point and latent heat were obtained using differential scanning calorimetry (DSC, TA SDT-Q600). The thermal conductivity was derived from the laser flash (LFA, NETZSCH LAF467 HyperFlash) measurement.

3. MD simulation

3.1 *Models set up*

The model of PEG was obtained from the Cambridge Crystallographic Data Centre (CCDC) (Fig.2a). For FDU-15, we got the model by digging holes in amorphous carbon via material studio software (Fig.2b). From the atomic level, the mesoporous carbon is amorphous and short-range disordered, but the arrangement of the pores is highly organized in long-range, and the pore size is within a narrow distribution, so it also has certain characteristics of crystals[31]. Their crystal information can be directly obtained by XRD.

(a) (b)

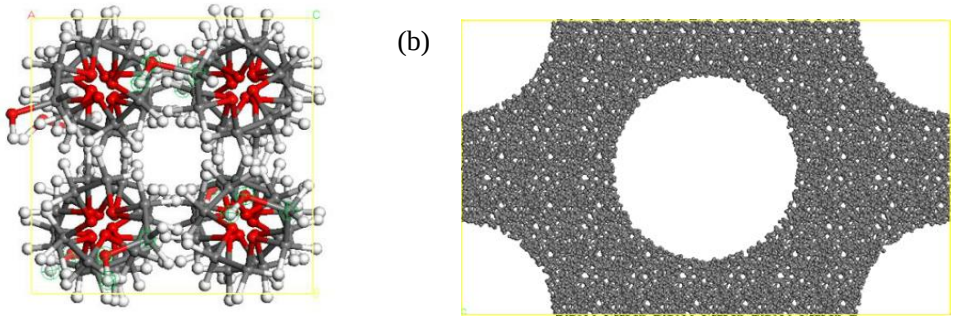

Fig.2 Simulation models of (a) PEG and (b) FDU-15 (Red：oxygen; white：hydrogen; grey：carbon)

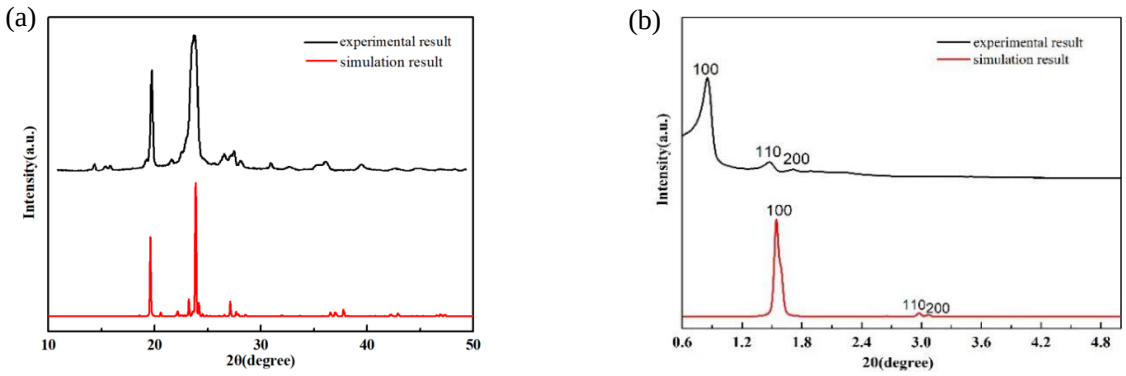

Fig.3 XRD patterns of (a) PEG and (b) FDU-15

As shown in Fig. 3, both PEG and FDU-15 show their unique peaks. Especially, there are three typical peaks in the XRD diagram of FDU-15 under experimental and simulated conditions, belonging to the (100), (110) and (200) crystal plane diffraction of the hexagonal system, respectively. According to the Bragg equation, the corresponding interplanar spacing values for experiments and simulation are calculated to be 10.38 nm, 5.96 nm, 5.13 nm and 5.7 nm, 3.25 nm, 2.88 nm, respectively, and both of the relative proportions are in accordance with 1: $(1/\sqrt{3})$:(1/2)[32]. The results proved that the mesoporous carbon model has a two-dimensional hexagonal ordered structure, and set-up models for MD simulation are physically logical.

However, MD modeling is relatively time-consuming due to the massive atoms in the composite system. Considering that the atoms on the inner wall of the channel possess the main effects on PEG, we only retain the atoms within this part (with the box size of 46 Å×46 Å×136 Å) according to the simplified concept (Fig. 4b)[33].

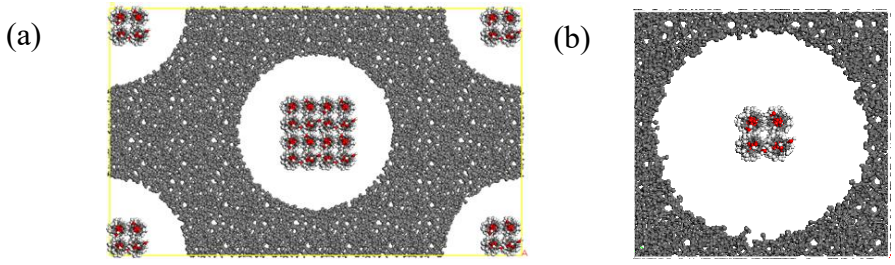

Fig. 4 (a) initial and (b) simplified model of PEG/FDU-15 composite

3.2 *Force field*

Fig. 5 shows the atomic types of FDU-15 and PEG. The force field of the FDU-15 and PEG system was described by Tersoff [34] and PCFF [35] force field, respectively. The L-J (Lennard-Jones) potential[36] was used to predict the interaction between FDU-15 and PEG, and the L-J parameters were determined by Lorentz-Berthelot mixed rule. The long-range Coulomb interaction was calculated based on the Ewald summation method. The computation was carried out with periodic boundary conditions, using a time step of 0.1 fs and a total simulation time of 200 ns.

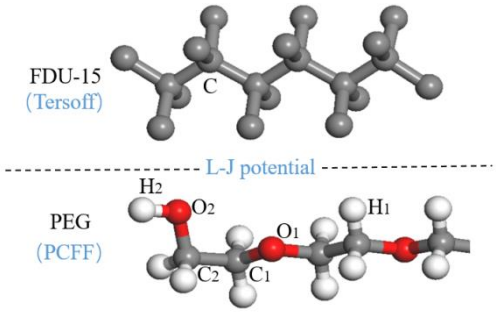

Fig. 5 Atomic types of FDU-15 and PEG

4. Results and discussion

4.1 *Structural characterization*

TEM image (Fig. 6a) shows the 2D well-organized hexagonal structure of mesoporous carbon FDU-15. The XRD characteristic peak for pure PEG located at 19.9° and 23.3° (2θ) in Fig. 6b, and the wide-angle peak of FDU-15 at 22.0° and 43.0° identifies its amorphous structure, and small-angel peaks show a hexagonal pore arrangement of FDU-15 as stated above.

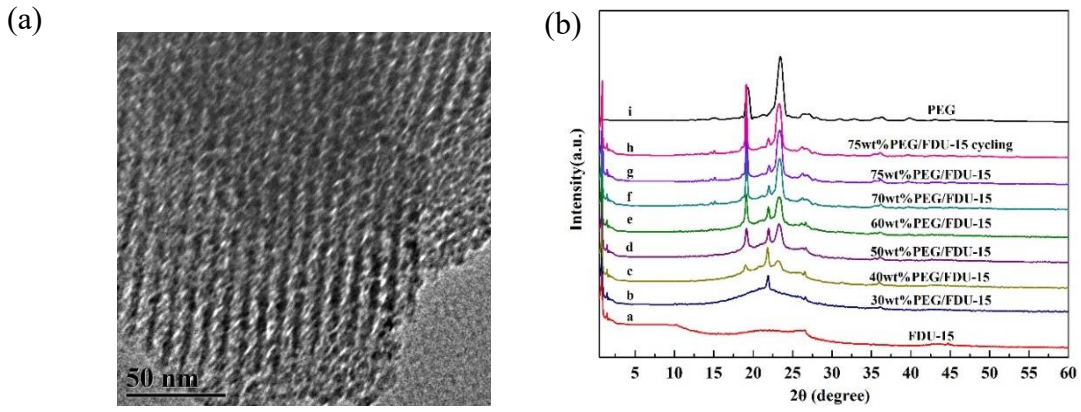

Fig. 6 (a)TEM image of FDU-15 and (b) XRD patterns of PEG, FDU-15 and the composites

After compounding, the peak of PEG gets stronger with increased loading, while a decline for that of FDU-15. For composites, all characterization peaks were inherited from parent materials without any new peaks appearing, indicating that the crystal structure of PEG is not affected by the skeleton FDU-15. Fig. 7 shows the FT-IR of FDU-15, PEG and their composites. For FDU-15, the absorption vibration at 3433 cm^{-1} is attributed to the stretching vibration of the O-H bond of the adsorbed water, the absorption vibration at 1626 cm^{-1} represents the stretching vibration of the C=C bond in the surface aromatic structure, and the absorption vibration at 1408 cm^{-1} is a C-H bond stretching vibration. In addition, there are many characteristic vibrations that appeared at 943, 1106, 1244, 1345, 1459, 2872, and 3433 cm^{-1} referring to a pure PEG. Specifically, the vibrations at 3433 cm^{-1} and 1106 cm^{-1} are corresponded to the stretching vibration of the O-H and C-O bonds, respectively. While the vibrations at 2872 cm^{-1} and 943 cm^{-1} indicate the stretching vibration of the $-CH_2$ group. Moreover, we can see that there is still no new absorption vibration of the composite even at 75 wt% loading of PEG, and vibrations from parent materials are all preserved, which certifies that there is only physical combination of the skeleton and the PEG, rather than a chemical relationship.

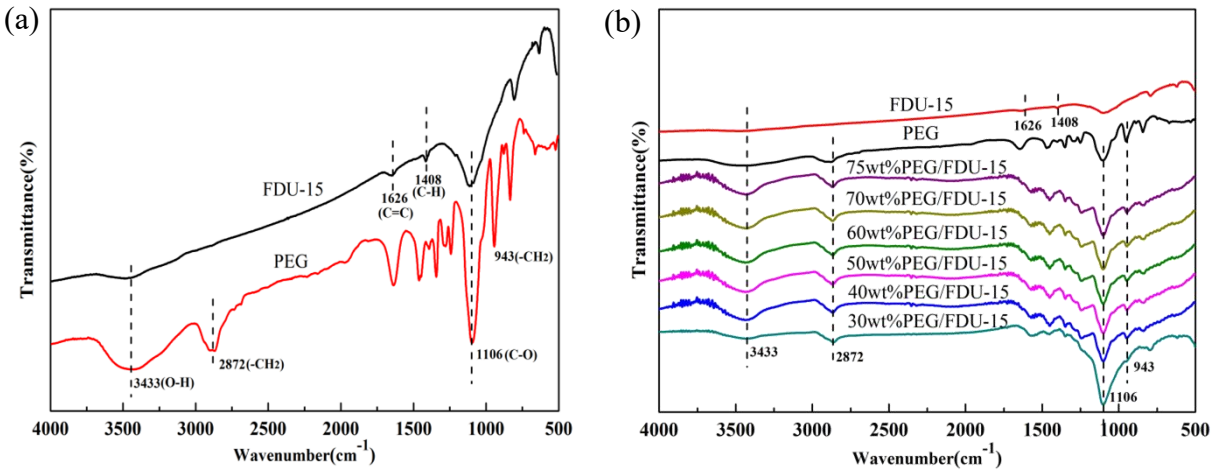

Fig. 7 FT-IR of (a) FDU-15, PEG and (b) the composites with different loading

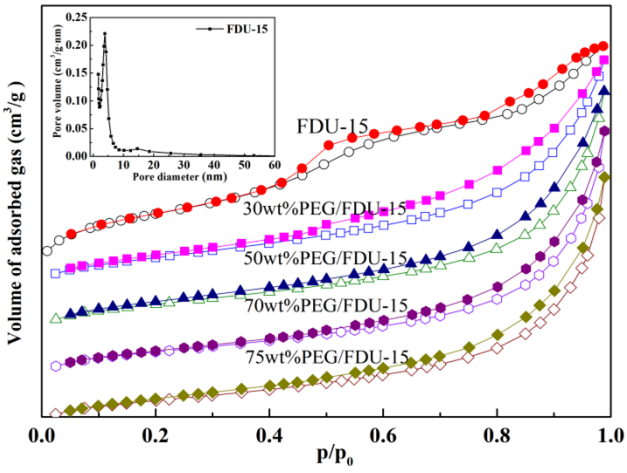

Fig. 8 Nitrogen adsorption-desorption isotherms of samples and pore size distribution of substrate (insert).(empty: adsorption isotherm, solid: desorption isotherm.)

Nitrogen adsorption-desorption isotherms of FDU-15 and PEG/FDU-15 composites were displayed in Fig. 8, as well as the pore size distribution curve of the substrate (inset of Fig. 8) and composites (**Supporting information Figure S1**). The skeleton FDU-15 shows the type IV isotherms. In the region with low P/P_0 (P/P_0 <0.4), since nitrogen forms monomolecular and multi-molecular adsorption on the wall, the nitrogen adsorption amount increases gradually with the increase of P/P_0. In the middle P/P_0 region (P/P_0 >0.4), capillary condensation occurs in the narrower mesoporous channels, resulting in a larger increase in the nitrogen adsorption amount. Furthermore, the nitrogen adsorption capacity increased sharply in the high P/P_0 region (P/P_0 =0.8-1.0), indicating that agglomeration may

occur between the particles during the synthesis of the material, resulting in a certain number of macropores. With the filling of PEG, more and more pores are occupied, the composite exhibits a type II isotherm. The structural parameters of FDU-15 and PEG/FDU-15 composites were summarized in Table 2. The specific surface area of pure FDU-15 is 898 m^2/g, and the total pore volume is 0.89 cm^3/g. When the PEG loading increases to the highest 75 wt%, the specific surface area and pore volume of the composite are reduced to 40 m^2/g, 0.13 cm^3/g, respectively. The decrease of total pore volume proves that the PEG was adsorbed into the pore structure. In addition, the SEM image shows that after compounding, the basic morphology of FDU-15 was maintained, and no excessive PEG attaching on the surface of FDU-15. The porous structure of FDU-15 prevents the leakage of liquid PEG due to capillary action and surface tension, so that PEG molecules can be anchored in the pores (**Supporting information Figure S2**).

Table 2 Structural parameters of FDU-15 and PEG/FDU-15 composites

Samples	Pore volume cm^3/g	Average pore size nm
FDU-15	0.89	4.84
30 wt% PEG/FDU-15	0.29	1.18
50 wt% PEG/FDU-15	0.17	1.19
70 wt% PEG/FDU-15	0.15	1.19
75 wt% PEG/FDU-15	0.13	1.19

4.2 *Measurement of phase change characteristics*

As can be seen from Fig. 9, there will be oil stains on the filter paper when PEG is overloaded. Hence, the maximum loading of using FDU-15 to pack PEG is derived to be 75wt%, which is superior to that of the mesoporous carbon composite PCMs SA/CMK-3 (46 wt%)[24] and mesoporous silica composite PCMs PEG/MCM-41-NH_2 (60 wt%)[22].

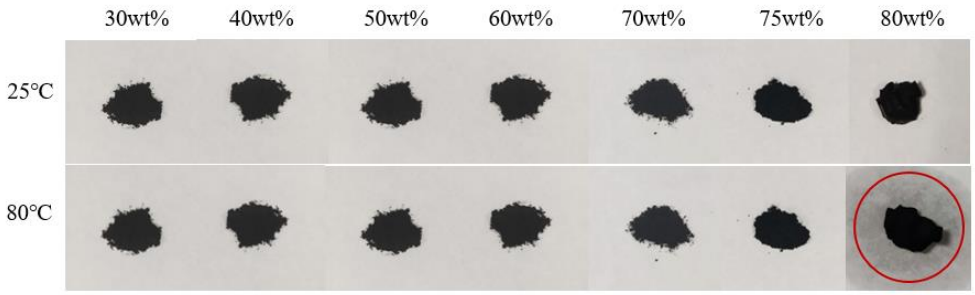

Fig. 9 Leakage test of PEG/FDU-15 composite

The melting point and latent heat were further obtained by DSC. The test temperature of the instrument can be from room temperature to 1500℃. The accuracy of enthalpy measurement is ±2%, the temperature accuracy is 0.1℃, and the sensitivity of DSC is 1 μW. Only when the filling reaches 40 wt%, the PEG begins to phase change within FDU-15, therefore releases the fusion enthalpy. In addition, the latent heat of the composite gradually grows with the increase of PEG mass percentage (Fig.10 and Table 3).

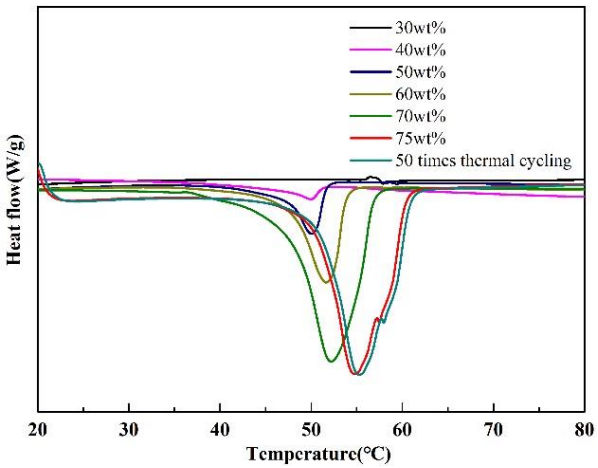

Fig. 10 Heat flow with the temperature of PEG/FDU-15

Table 3 Measurement results of phase change characteristics of PEG/FDU-15 composites

Sample	PEG loading wt%	T_m/ T_f ℃	$\Delta H_m/\Delta H_f$ J/g	Theoretical $\Delta H_m/\Delta H_f$ J/g	θ %	E %
1	100 (Pure PEG)	52.48/19.18	153.0/151.46	-/-	-/-	-

2	30	-/-	-/-	45.9/45.44	-/-	-
3	40	46.00/27.06	5.18/3.45	61.2/60.58	8.5/5.7	7.1
4	50	46.93/27.35	15.47/8.85	76.5/75.73	20.2/11.7	16
5	60	47.62/32.53	31.47/18.14	91.8/90.88	34.3/20.0	27.2
6	70	47.55/31.29	74.75/68.85	107.1/106.02	69.8/64.9	67.4
7	75	50.45/30.23	81.76/80.39	114.75/113.60	71.3/70.8	71.0
8	75(50 cycles)	50.87/30.14	81.32/80.21	114.75/113.60	70.9/70.6	70.7

We use crystallization ratio θ reflects the existing state of PEG inside the pores, and heat storage efficiency E is used to investigate the thermal storage capacity:

$$\theta = \frac{H_S}{wt\% \times H_{pure}} \times 100\% \quad (1)$$

$$E = \frac{\Delta H_{m,comp} + \Delta H_{f,comp}}{wt\% \times (\Delta H_{m,PCM} + \Delta H_{f,PCM})} \times 100\% \quad (2)$$

Where $\Delta H_{m,comp}$ and $\Delta H_{m,PCM}$ represents the melting latent heat of composite materials and pure PEG, respectively. $\Delta H_{f,comp}$ and $\Delta H_{m,PCM}$ stands for the cooling enthalpies of composites and PEG, respectively. Hs is the measured latent heat, wt% represents the mass percentage of PEG, and H_{pure} is regarded as the theoretical enthalpy of pure PEG. It is interesting to see a reduced supercooling of PEG after nanoconfinement (Fig. 11a). The gap between melting point and freezing point narrows to 20℃ while more than 30℃ for pure PEG. This is because the huge specific surface area of FDU-15 provides a large number of nucleation sites for heterogeneous nucleation of PEG, which is helpful for the crystallization of PEG. It's a good sight for its practical application especially during new energy storage such as solar energy[37]. The crystallization ratio and heat storage efficiency of PEG are more than 70% at the maximum loading (Fig. 11b), but still a large gap with 100%. It is a kind of very general phenomenon in nanoporous composite PCMs[22-24, 38]. The confined PEG attached to the wall could easily form an amorphous structure that was responsible for the loss of crystallization. It seems like that mesoporous carbon FDU-15 has a better condition for PEG crystallization comparing with same-

structured MCM-41 of ~60% PEG crystallization ratio at a maximum[22]. Moreover, 75 wt% PEG/FDU-15 also presented good thermal stability after 50 times cycling, the melting point, fusion enthalpy, crystallization ratio and heat storage efficiency of PEG hardly change. We further compared the thermal properties of several commonly used composite phase change materials (silicon-based, carbon-based, and metal-organic frameworks). As shown in Fig. 11c, PEG/FDU-15 composite material exhibits a better heat storage performance.

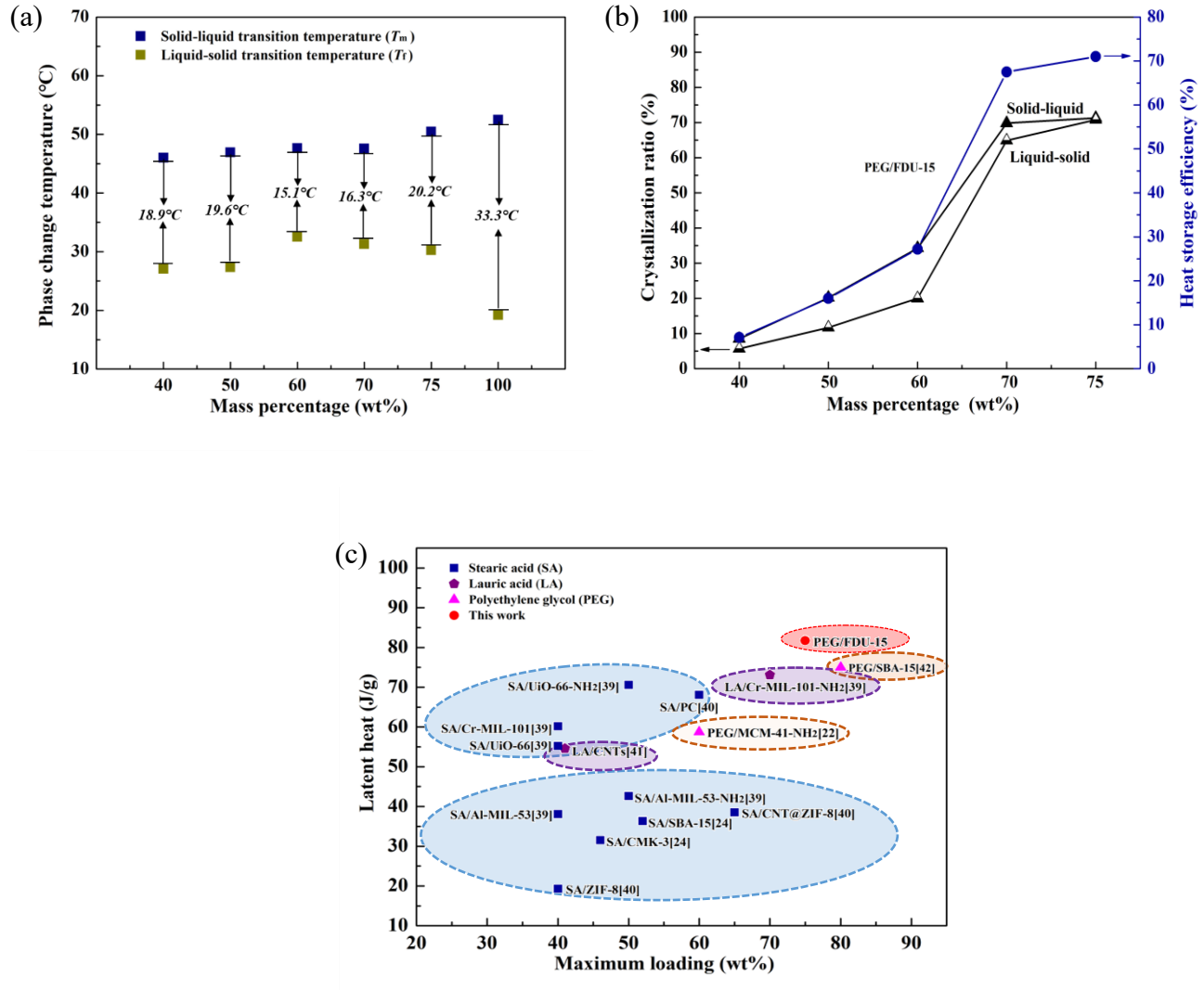

Fig. 11 (a) Phase transition temperature and supercooling extent of pure PEG and composite, (b) crystallization ratio and heat storage efficiency of PEG/FDU-15 and (c) maxing loading and latent heat of composite PCMs with

different skeletons.[22, 24, 39-42]

4.3 *Analysis of phase change mechanisms*

The DSC results (Table 3) show that the melting point of the composites is lower than that of the pure PEG (sample 1). Many studies have indicated that the phase change characteristics of PCMs in confined spaces are different from their bulks[43,44], but the underlying mechanism is quite complicated which is associated with nano-size effect and interfacial effect, yet far from being revealed. Here, we used the radius of gyration to identify the difference between free PEG and confined PEG, further reflecting the melting point. The formula for calculating the radius of gyration (R_g) is as follow:

$$R_g = \sqrt{\frac{\sum_i m_i r_i^2}{\sum_i m_i}} \tag{3}$$

Where m_i represents the atom mass, r_i is the distance between the atom i and the centroid. It can be seen from Fig. 12 that the R_g of the PEG in the confined space (red line) is smaller than that of the bulk PEG (black line), which means the PEG segments get more flexible within FDU-15 channels results in a lower melting point[45]. That is to say a much easier breaking down the structure of the confined PEG.

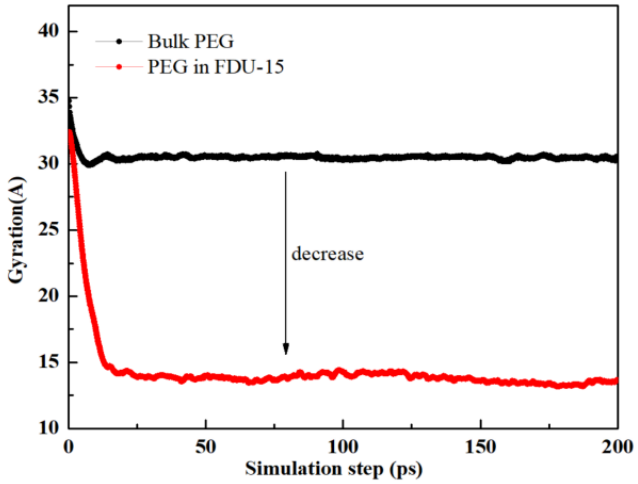

Fig.12 Radius of gyration of PEG before and after compounding

Taking the center of the mesopore as the origin and the radial direction as the abscissa, the position

distribution of the PEG atoms was obtained, as shown in Fig. 13. Some atoms of PEG distribute adhere to the wall. We can determine that these adherent atoms have a strong interaction with the skeleton, and no phase change occurs. The result is consistent with the DSC experimental results.

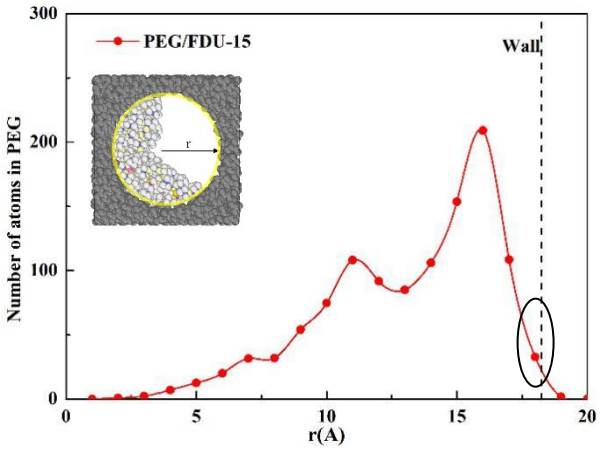

Fig.13 Atomic distribution of PEG in FDU-15

According to our previous conclusions[46,47], strong guest-host interaction takes a negative effect on the crystallization of confined PCM. In Fig.14, there is a dramatic reduction in interaction energy between PEG molecules and FDU-15, comparing with PEG and MCM-41 counterparts. This might provide evidence for a higher crystallization ratio of PEG in FDU-15.

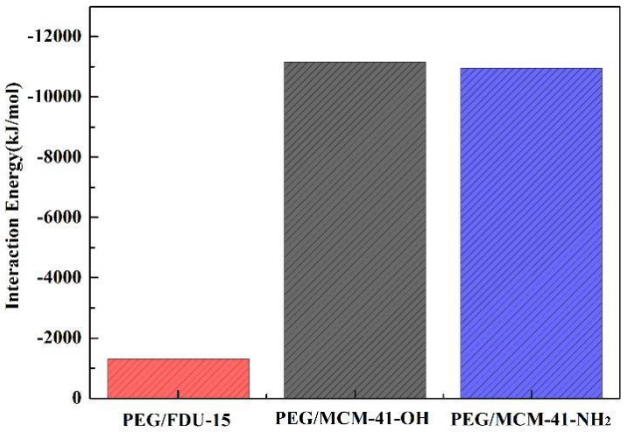

Fig.14 Guest-host interaction energy of mesopore-based composite PCMs

4.4 *Thermal conductivity*

4.4.1 *LFA measurement*

The sample is pressed into a sheet with a thickness of h (1-2 mm) in a mold (r = 6.4 mm). The volume v of the sample is obtained according to Equation 4. Then weigh the mass of the sample and obtain its density according to Equation 5. The thermal diffusivity and specific heat at temperature T are obtained by the laser flashing (LFA) method. Finally, the thermal conductivity of the sample could be obtained according to Equation 6.

$$v = \pi r^2 h \tag{4}$$

$$\rho = \frac{m}{v} \tag{5}$$

$$\lambda(T) = \alpha(T) \times C_p(T) \times \rho(T) \tag{6}$$

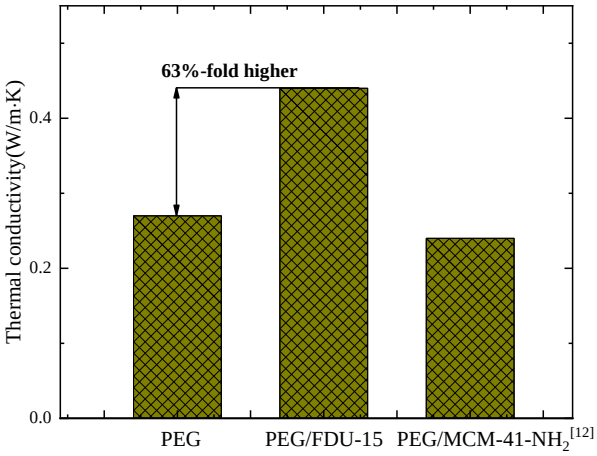

Fig.15 Thermal conductivities of PEG and its composites

The results are displayed in Fig. 15. The thermal conductivity of PEG/FDU-15 with 75 wt% PEG is 0.44 W/(m·K), which is 63%-fold higher than that of pure PEG (0.27 W/(m·K)). It also shows prominent advantage over same-structured silicon-based composite PEG/MCM-41(0.24 W/(m·K)[22]). The disordered porous carbon with a certain degree of graphitization may benefit to the thermal performance (**Supporting information Figure S3**). Besides, the thermal conductivity of PEG/FDU-15 is comparative to that of PEG/HPC (0.42 W/(m·K))[30]. Hierarchical porous carbon (HPC) with an extremely high loading of PEG (92.5 wt%) is expected to have a higher thermal conductivity as less confined air within the pores.

4.4.2 *Vibration dynamic density*

We are trying to explain the increase of thermal conductivity after guest-host assembling via a micro-aspect. The vibration of atoms before and after compounding was investigated by calculating the Vibrational Density of States (VDOS). The VDOS of a class atom is obtained by the Fourier transform and the weighting factor of its velocity autocorrelation function (VACF). The calculation formula is as follows[48]:

$$D_{p,\beta}(t) = c_\beta \int_0^\tau \Gamma_\beta(t)\cos(\omega t)dt \tag{7}$$

$$\Gamma_\beta(t) = \sum_i^{N_\beta} \langle \mu_{i\beta}(t)\cdot\mu_{i\beta}(0)\rangle / \sum_i^{N_\beta} \langle \mu_{i\beta}(0)\cdot\mu_{i\beta}(0)\rangle \tag{8}$$

Where ω is frequency, Γ_β is the velocity of the atom of class β, and ⟨ ⟩ is the time average. The VDOS of PEG, FDU-15 and the contribution of the respective atomic vibrations to heat transfer are shown in Fig.16.

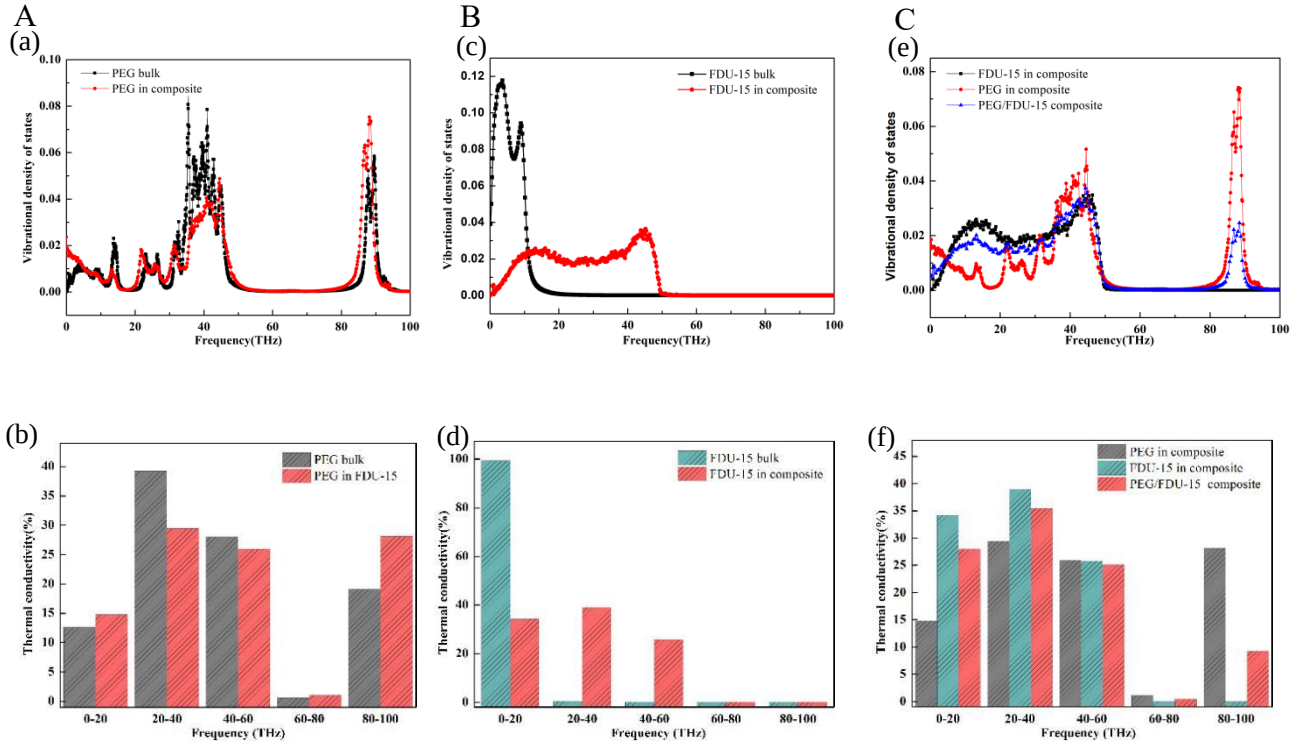

Fig. 16 The VDOS of the material (a, c, e) before and after compounding and the contribution of the respective atomic vibrations to heat transfer (b, d, f) (A: PEG system; B: FDU-15 system; C: PEG/FDU-15 composites.

Before compounding, the main vibration peaks of the pure PEG fall into the range of 30-50 THz and

80-100 THz (Fig.16A(a)), identifying the greatest contribution to heat transfer. For FDU-15, the main contributor to heat transfer locates in the low frequency range 0-20 THz (Fig.16B(c)). Once the two materials assembled, the atomic vibration of PEG itself is suppressed (Fig.16A(a)), but the filling of PEG stimulates the atomic vibration of the intermediate frequency within FDU-15, causing the main vibration peak shifts from low frequency to intermediate frequency region. Thus, the atomic vibration of the skeleton and PCM ends up with a better match at middle frequency band (Fig. 16C(f)), which might be responsible for the promotion of the thermal conductivity.

4.4.3 *Overlapping energy*

Based on the qualitative analysis of VDOS, this paper introduces the concept of overlapping energy, and quantitatively calculates the overlap energy between each two bonding atoms (overlap phonon energy). The formula is as follow [49]:

$$E_{overlap} \int g_0(\nu) \frac{\mathrm{h}\nu}{\exp\left(\frac{\mathrm{h}\nu}{\mathrm{k_B}T}\right)-1} \mathrm{d}\nu \tag{9}$$

Where $g_0(\nu)$ is the overlap region of VDOS, h is the Planck constant, ν is the frequency, $\exp(\mathrm{h}\nu/\mathrm{k_B}\mathrm{T})-1$ is the Boltzmann distribution; T is the absolute temperature, and $\mathrm{K_B}$ is the Boltzmann constant. The higher the overlap energy, the more coordinated the vibration between the two atom types, thus the more favorable the transfer of energy.

Since PEG is a polymer with a C-C-O segment repetitive structure, the C-O bond is the “weak link” of energy transfer along the chain. Therefore, we calculated the overlap energy between C-O to evaluate the effect of guest host combination on energy transfer.

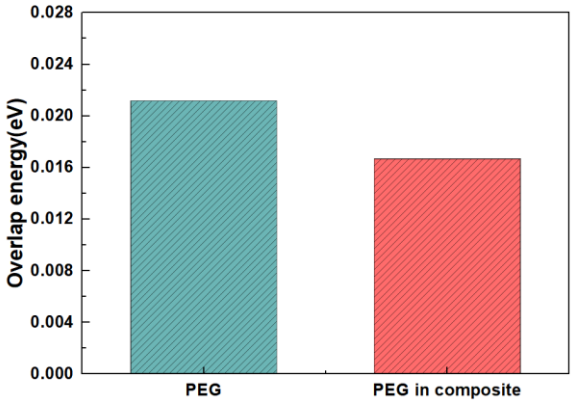

Fig. 17 The overlap energy between C-O atoms in PEG before and after compounding

As shown in Fig. 17, we can see that the overlap energy of C-O in the composite material is much lower than that of the pure bulk material, indicating that the FDU-15 pore structure makes the PEG chain irregularly arranged therefore hinders the phonon transport. As a result of the mismatch between the atomic vibrations, the heat transfer along PEG chains start to suffer. This result also coincides with the above VDOS. It seems like that the promotion of thermal conductivity of composite should be attributed to the frequency shift of FDU-15 after assembly, resulting in an improved matching with PEG, even though the guest-host merging causes a loose of heat transfer ability of PEG.

4.4.4 *Local heat flow*

For further proof, we select two layers of atoms (64-72 Å) in the longitudinal (z) direction of the skeleton FDU-15, calculate the local heat flow of the material, and then project the local heat flow of the selected atom to the XY plane. Considering that the inner surface of the skeleton channel has the greatest influence on the PCM material, only the information from carbon atoms on the inner surface of the channel is output. As shown in Fig. 18, after the PEG is filled in, the interaction between PEG and FDU-15 enhances the local heat flow of the composite as a whole, which is direct evidence for ameliorative heat transfer.

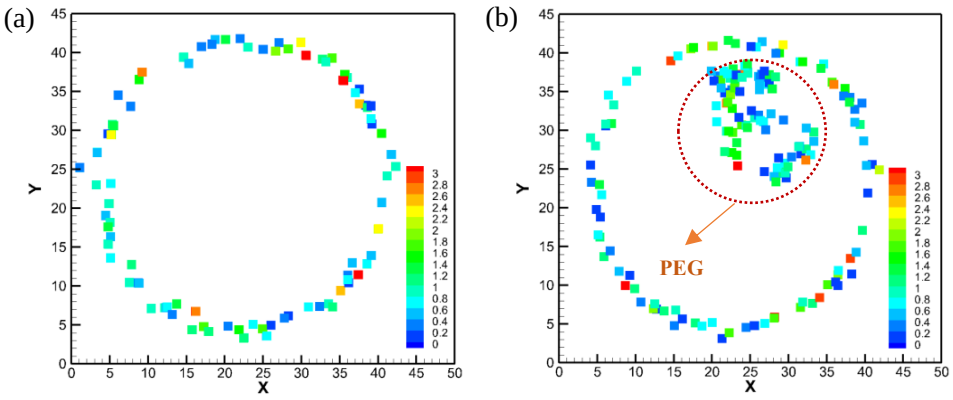

Fig. 18 Projection of localized heat flux of (a) FDU-15 and (b) PEG/FDU-15 on X-Y plane

5. Conclusions

A kind of mesoporous carbon FDU-15 was first used to pack phase change PEG as a novel shape-stabilized phase change material. The pore morphology was observed by TEM and the chemical composition of the materials was characterized by FT-IR. The melting/freezing point and latent heat of the composites with different loading were measured by DSC. For the phenomena in the experiment, the phase change and the heat transfer mechanism were explained by molecular dynamics simulation. The main conclusions of the full text are as follows:

(1) In terms of phase change, experiments show that the maximum loading of PEG/FDU-15 could be up to 75 wt%, the corresponding crystallization ratio is over 70%. The latent heat increases with the increase of PEG percentage. The simulation analysis indicated that the flexibility of the segment of the PEG after assembly was reduced, thus the melting point is slightly lower than pure PEG. Partially attached-wall atoms exist in the pores form an amorphous configuration with no phase change, resulting in a loose of latent heat.

(2) In terms of heat transfer, for the PEG, the vibration of the phonon in the intermediate frequency range after the composite is slightly lowered down. It can be verified by the reduced overlapping energy of C-O, the atomic vibration with less coordination. For FDU-15, the introduction of the PEG excites

the vibration of the atoms shift to the middle frequency domain, then enables the skeleton and PEG vibrate at a similar frequency. It can be seen from the local heat flow that the filling of PEG reinforces the heat transfer, and the thermal conductivity of the composite is increased by more than 60% compared with the pure PCM.

(3) Compared with same-structured PEG/MCM-41 and other mesoporous carbon, PEG/FDU-15 behaves an improved loading, crystallization and heat transfer performance. The choice of a skeleton to pack PCM matters a lot to the overall thermal properties of the derived composite, therefore provides us with higher flexibility to design mesopore-based shape-stabilized composite PCM according to actual needs.

ACKNOWLEDGMENTS

This work is financially supported by the China National Key Research and Development Plan Project (No. 2018YFA0702300), the National Natural Science Foundation of China (No. 51876007), the Beijing Natural Science Foundation (No.3192022), the Fundamental Research Funds for the Central Universities (FRF-TP-19-007B1, FRF-TP-19-002B2) and China Scholarship Council.

References

[1] Yu M, Hong S H. Supply–demand balancing for power management in smart grid: A Stackelberg game approach[J]. *Applied energy*, **2016**, 164: 702-710.

[2] Wu D, Wen W, Chen S, Zhang H L. Preparation and Properties of a Novel Form-Stable Phase Change Material Based on a Gelator[J]. *J. Mater. Chem. A,* **2015**, *3*, 2589-2600.

[3] Tan F L, Tso C P. Cooling of mobile electronic devices using phase change materials[J]. *Applied Thermal Engineering*, **2004**, 24(2-3):159-169.

[4] Nayak K C, Saha S K, Srinivasan K, Dutta P. A numerical model for heat sinks with phase change materials and thermal conductivity enhancers[J]. *International Journal of Heat and Mass Transfer*, **2006**, 49(11-12):1833-1844.

[5] Kim T Y, Hyun B S, Lee J J, Rhee J. Numerical study of the spacecraft thermal control hardware combining solid–liquid phase change material and a heat pipe[J]. *Aerospace Science and Technology*, **2013**, 27(1):10-16.

[6] Wu W F, Liu N, Cheng W L, Liu Y. Study on the effect of shape-stabilized phase change materials on spacecraft thermal control in extreme thermal environment[J]. *Energy Conversion and Management*, **2013**, 69:174-180.

[7] Su W, Darkwa J, Kokogiannakis G. Review of solid–liquid phase change materials and their encapsulation technologies[J]. *Renewable and Sustainable Energy Reviews*, **2015**, 48: 373-391.

[8] Sharma R K, Ganesan P, Tyagi V V, Metselaar H S C, Sandaran S C. Developments in organic solid–liquid phase change materials and their applications in thermal energy storage[J]. *Energy Conversion and Management*, **2015**, 95: 193-228.
[9] Mohamed S A, Al-Sulaiman F A, Ibrahim N I, Zahir M H, Al-Ahmed A, Saidur R, et al. A review on current status and challenges of inorganic phase change materials for thermal energy storage systems[J]. *Renewable and Sustainable Energy Reviews*, **2017**, 70: 1072-1089.
[10] Milian Y E, Gutierrez A, Grageda M, Ushak S. A review on encapsulation techniques for inorganic phase change materials and the influence on their thermophysical properties[J]. *Renewable and Sustainable Energy Reviews*, **2017**, 73: 983-999.
[11] Feng D L, Feng Y H, Qiu L, Li P, Zang Y Y, Zhang X X, et al. Review on nanoporous composite phase change materials: Fabrication, characterization, enhancement and molecular simulation[J]. *Renewable and Sustainable Energy Reviews*, **2019**, 109: 578-605.
[12] Pasupathy A, Velraj R, Seeniraj R. Phase change material-based building architecture for thermal management in residential and commercial establishments[J]. *Renewable and Sustainable Energy Reviews*, **2008**, 12(1): 39-64.
[13] Zhang X, Yin Z, Meng D, Huang Z H, Wen R L, Huang Y T, et al. Shape-stabilized composite phase change materials with high thermal conductivity based on stearic acid and modified expanded vermiculite[J]. *Renewable Energy*, **2017**, 112: 113-123.
[14] Wang W T, Tang B T, Ju B Z, Gao Z M. Fe_3O_4-functionalized graphene nanosheet embedded phase change material composites: efficient magnetic-and sunlight-driven energy conversion and storage[J]. *Journal of Materials Chemistry A*, **2017**, 5(3): 958-968.
[15] Nada S, Alshaer W. Comprehensive parametric study of using carbon foam structures saturated with PCMs in thermal management of electronic systems[J]. *Energy Conversion and Management*, **2015**, 105: 93-102.
[16] Zhang Q, Liu J, Yuan K J, Zhang Z G, Zhang X W, Fang X M. A multi-controlled drug delivery system based on magnetic mesoporous Fe3O4 nanopaticles and a phase change material for cancer thermo-chemotherapy[J]. *Nanotechnology*, **2017**, 28(40): 405101.
[17] Boomsma K, Poulikakos D. On the effective thermal conductivity of a three- dimensionally structured fluid-saturated metal foam[J]. *International Journal of Heat and Mass Transfer*, **2001**, 44(4):827-836.
[18] Qi G Q, Yang J, Bao R Y, Xia D Y, Cao M, Yang W, et al. Hierarchical graphene foam-based phase change materials with enhanced thermal conductivity and shape stability for efficient solar-to-thermal energy conversion and storage[J]. *Nano Research*, **2017**, 10(3):802-813.
[19] Wu M, Fujiu T, Messing G L. Synthesis of cellular inorganic materials by foaming sol-gels[J]. *Journal of Non Crystalline Solids*, **1990**, 121(1-3):0-412.
[20] Maria Chong A S, Zhao X S. Functionalization of SBA-15 with APTES and Characterization of Functionalized Materials[J]. *The Journal of Physical Chemistry B*, **2003**, 107(46):12650-12657.
[21] Wiktor C, Turner S, Zacher D, R A Fischer, G V Tendeloo. Imaging of intact MOF-5 nanocrystals by advanced TEM at liquid nitrogen temperature[J]. *Microporous and Mesoporous Materials*, **2012**,162:131–5.
[22] Wang C, Feng Y H, Feng D L, Wang G, Zhang X X. Thermophysical properties and modified groups mechanism of silicon- based composite phase change materials[J]. *Journal of Engineering*

Thermophysics, **2019**,40: 1180-1187.
[23] Wang J J, Yang M, Lu Y F, Jin Z K, Dong W J, Wang G, et al. Surface functionalization engineering driven crystallization behavior of polyethylene glycol confined in mesoporous silica for shape-stabilized phase change materials[J]. *Nano Energy*, **2016**, 19:78–87.
[24] Kadoono T, Ogura M. Heat storage properties of organic phase-change materials confined in the nanospace of mesoporous SBA-15 and CMK-3[J]. *Physical Chemistry Chemical Physics*, **2014**, 16(12): 5495-5498.
[25] Wu Z X, Webley P A, Zhao D Y. Comprehensive study of pore evolution, mesostructural stability, and simultaneous surface functionalization of ordered mesoporous carbon (FDU-15) by wet oxidation as a promising adsorbent[J]. *Langmuir*, **2010**, 26(12): 10277-10286.
[26] Yan Y, Wei J, Zhang F Q, Meng Y, Tu B, Zhao D Y. The pore structure evolution and stability of mesoporous carbon FDU-15 under CO2, O2 or water vapor atmospheres[J]. *Microporous and Mesoporous Materials*, **2008**, 113(1-3): 305-314.
[27] Wang K Q, Yang H, Zhu L, Ma Z S, Xing S Y, Lv Q, et al. Direct electron transfer and electrocatalysis of glucose oxidase immobilized on glassy carbon electrode modified with Nafion and mesoporous carbon FDU-15[J]. *Electrochimica Acta*, **2009**, 54(20): 4626-4630.
[28] Wang C Y, Wang W, Xin G B, Li G L, Zheng J, Tian W H, et al. Phase change behaviors of PEG on modified graphene oxide mediated by surface functional groups[J]. *European Polymer Journal*, **2016**, 74: 43-50.
[29] Feng L L, Zheng J, Yang H Z, Guo Y L, Li W, Li X G. Preparation and characterization of polyethylene glycol/active carbon composites as shape-stabilized phase change materials[J]. *Solar Energy Materials and Solar Cells*, **2011**, 95: 644-650.
[30] Tang J, Yang M, Dong W J, Yang M, Zhang H, Wang G, et al. Highly porous carbons derived from MOFs for shape-stabilized phase change materials with high storage capacity and thermal conductivity[J]. *RSC Advances*, **2016**, 6: 40106-40114.
[31] Huang Z, Huang C L, Wu D X , Rao Z H. Influence of chemical bonding on thermal contact resistance at silica interface: A molecular dynamics simulation[J]. *Computational Materials Science*. **2018**,149:316-23
[32] Trick K A, Saliba T E. Mechanisms of the pyrolysis of phenolic resin in a carbon/phenolic composite[J]. *Carbon*, **1995**, 33(11): 1509-1515.
[33] Chang S C, Chien S Y, Chen C L, Chen C K. Analyzing adsorption characteristics of CO2, N2 and H2O in MCM-41 silica by molecular simulation[J]. *Applied Surface Science*, **2015**, 331:225-233.
[34] Lindsay L, Broido D A. Optimized Tersoff and Brenner empirical potential parameters for lattice dynamics and phonon thermal transport in carbon nanotubes and graphene[J]. *Physical Review B*, **2010**, 82(20):209903.
[35] Sun H, Mumby S J, Maple J R, Hagler A T. An ab Initio CFF93 All-Atom Force Field for Polycarbonates[J]. *Journal of the American Chemical Society*, **1994**, 116(7):2978-2987.
[36] Jones, J. E. On the Determination of Molecular Fields. II. From the Equation of State of a Gas[J]. Proceedings of the Royal Society A: Mathematical, *Physical and Engineering Sciences*, **1924**, 106(738):463-477.
[37] Tian Y, Zhao C Y. A review of solar collectors and thermal energy storage in solar thermal applications[J]. *Appl Energy*, **2013**,104:538–53.

[38] Wang Y M, Tang B T, Zhang S F. Single‐walled carbon nanotube/phase change material composites: sunlight‐driven, reversible, form‐stable phase transitions for solar thermal energy storage[J]. *Advanced Functional Materials*, **2013**, 23(35): 4354-4360.
[39] Luan Y, Yang M, Ma Q Q, Qi Y. Introduction of an organic acid phase changing material into metal–organic frameworks and the study of its thermal properties[J]. *Journal of Materials Chemistry A*, **2016**, 4(20): 7641-7649.
[40] Li A , Wang J J, Dong C, Dong W J, Dimberu G A, Chen X, et al. Core-sheath structural carbon materials for integrated enhancement of thermal conductivity and capacity[J]. *Applied Energy*, **2018**, 217:369-376.
[41] Feng Y H, Wei R Z, Huang Z, Zhang X X, Wang G. Thermal properties of lauric acid filled in carbon nanotubes as shape-stabilized phase change materials[J]. *Physical Chemistry Chemical Physics*. **2018**;20:7772-80.
[42] Feng L L, Zhao W, Zheng J, Frisco S, Song P, Li X G. The shape-stabilized phase change materials composed of polyethylene glycol and various mesoporous matrices (AC, SBA-15 and MCM-41)[J]. *Solar energy materials and solar cells*, **2011**, 95(12): 3550-3556.
[43] Zhang D, Tian S L, Xiao D Y. Experimental study on the phase change behavior of phase change material confined in pores[J]. *Solar Energy*, **2007**, 81(5): 653-660.
[44] Radhakrishnan R, Gubbins K E, Watanabe A, Kaneko K. Freezing of simple fluids in microporous activated carbon fibers: comparison of simulation and experiment[J]. *The Journal of chemical physics*, **1999**, 111(19): 9058-9067.
[45] Wang Y H, Wang W H, Zhang Z Q, Xu L C, Li P. Study of the glass transition temperature and the mechanical properties of PET/modified silica nanocomposite by molecular dynamics simulation[J]. *European Polymer Journal*, **2016**, 75: 36-45.
[46] Feng D L, Feng Y H, Zang Y Y, Li P, Zhang X X. Phase change in modified metal organic frameworks MIL-101 (Cr): mechanism on highly improved energy storage performance[J]. *Microporous Mesoporous Mater* **2019**,280:124–32.
[47] Feng D L, Feng Y H, Li P, Zang Y Y, Wang C, Zhang X X. Modified mesoporous silica filled with PEG as a shape-stabilized phase change material for improved thermal energy storage performance[J]. *Microporous Mesoporous Mater* **2020**,292:109756.
[48] Loong C K, Hinks D G, Vashishta P, Jin W, Kalia R K, Degani M H, et al. Phonon density of states and oxygen-isotope effect in Ba1−xKxBiO3[J]. *Physical Review B*, **1992**, 45(14): 8052-8064.
[49] Zhang X L, Jiang J W. Thermal conductivity of zeolitic imidazolate framework-8: A molecular simulation study[J]. *The Journal of Physical Chemistry C*, **2013**, 117(36): 18441-18447.